Supporting Information

Buchwald et al. 10.1073/pnas.1000993107

SI Text

Nanoliter Liquid Chromatography (nanoLC)-MS/MS. Dissolved crystals were digested with Trypsin and the peptides were separated by online nanoLC and analyzed by electrospray tandem mass spectrometry as described in ref. S1. Data analysis was performed with the MaxQuant software supported by Mascot as the database search engine for peptide identifications.

Surface Plasmon Resonance (SPR) Spectroscopy. SPR spectroscopy was performed at 25 °C using a BIAcore 3000 (GE Healthcare). Anti-GST antibody was immobilized on a CM5 chip using an amine coupling procedure with a 30 μg/mL antibody at 5 μL/min in 10 mM sodium acetate at pH 5.0. Approximately 10,000 response units (RUs) were immobilized on the chip. The anti-GST chips were then derivatized with 100–150 RUs of GST-tagged UPF3 in 40 mM Tris · HCl pH 7.5, 300 mM NaCl, and 1 mM DTT, with the addition of 3 mM $MgCl_2$ in case of the EJC or of 0.05% Tween 20 in case of UPF2 (running buffer). An anti-GST flow cell was used as control. Binding experiments were carried out at a flow rate of 30 μL/min in running buffer. The BIAcore 3000 evaluation software was used for analysis of the experimental data. The saturation binding values were fitted according to a one-site binding model using the Origin software.

1. Olsen JV, et al. (2010) Parts per million mass accuracy on an Orbitrap mass spectrometer via lock mass injection into a C-trap. *Mol Cell Proteomics* 4:2021

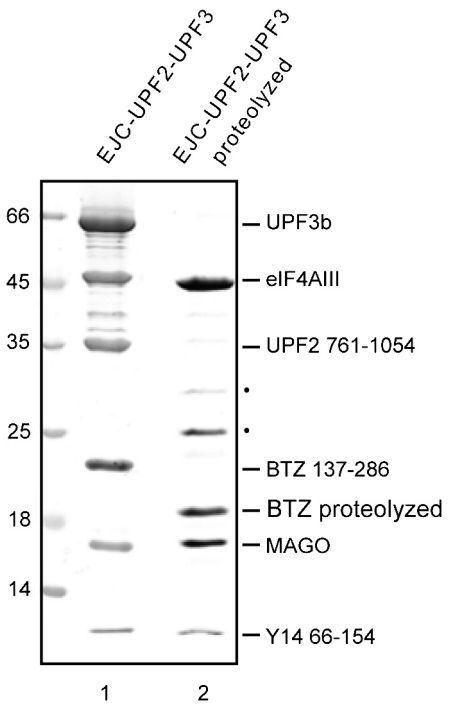

Fig. S1. Purification of a minimal complex of the exon junction complex (EJC) with UPF3b for crystallization. The peaks of the final size-exclusion chromatography purifications of the intact and proteolyzed EJC-UPF3b-UPF2 complexes were separated on a 10% (wt/vol) acrylamide SDS-PAGE gel (lanes 1 and 2, respectively) together with a protein marker (left lane), and stained with Coomassie. The corresponding protein constructs are labeled on the right. Crystals were obtained from the EJC-containing mixture in lane 2 (note that the presence of low molecular weight peptides is not assessed in this type of gel). Dots indicate fragments of Up-frameshift proteins (UPF) that peaked at a shoulder in the chromatogram and could not be separated from the peak fractions.

Data collection and refinement statistics	
Data collection	
Beamline	PXII
Wavelength (Å)	1.0
Space group	$P4_12_12$
Cell dimensions (Å)	a = b = 134.8, c = 227.2
Resolution range (Å)[1]	60 – 3.4 (3.58 – 3.40)
No. of Reflections	29550
Multiplicity[1]	10 (10)
$I/\sigma(I)$ [1]	7.4 (2.1)
R_{merge} (%)[1]	9.7 (36.2)
Completeness (%)[1]	100 (100)
Refinement statistics	
Resolution range (Å)	60 – 3.4
R_{work}	22.04
R_{free}	26.04
No. of atoms	11716
Protein atoms	11358
Nucleotide atoms	356
Magnesium	2
r.m.s.d. bonds (Å)	0.013
r.m.s.d. angles (°)	1.464
Ramachandran values	
Most favored (%)	95.5
Additionally allowed (%)	4.5
Disallowed (%)	0.0

[1]Values for highest resolution bin (3.58 – 3.40 Å) are given in brackets.

Fig. S2. Data collection and refinement statistics of the crystal structure of the minimal EJC-UPF3b complex.

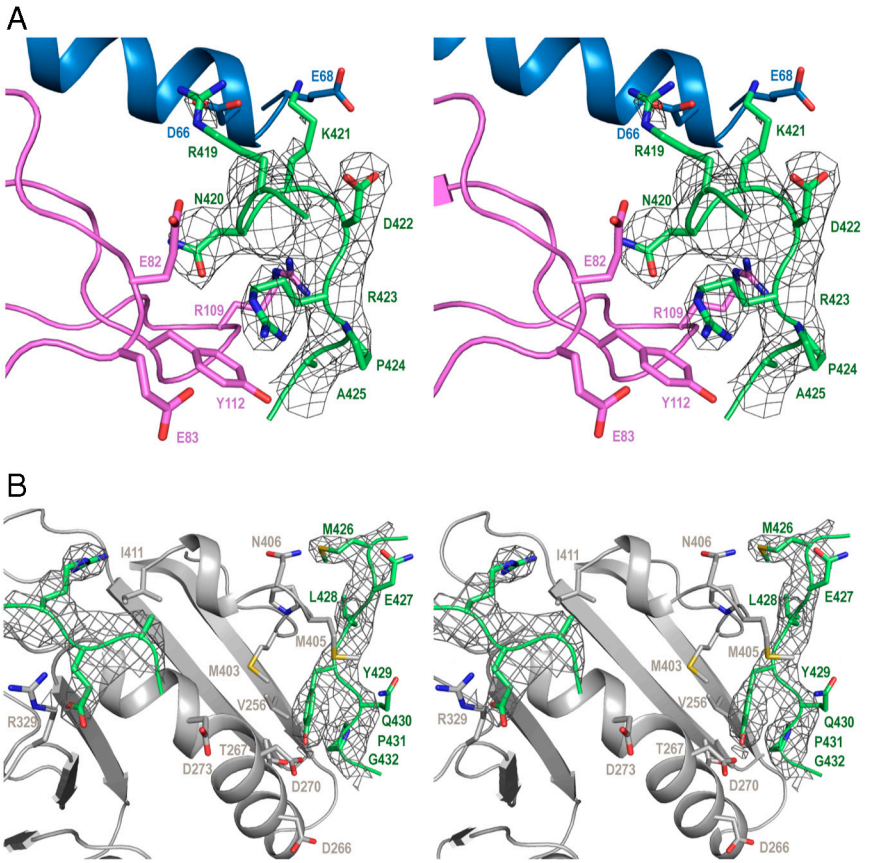

Fig. S3. Electron density map showing segments of the complex interface. (*A*) Stereo ribbon representation of the interaction between UPF3b and MAGO-Y14 (blue and pink, respectively) together with the 2fo-fc map, contoured at 1.0 s showing the electron density after UPF3b was modeled. The molecules are viewed in a similar orientation to that used in Fig. 2*B*. (*B*) Stereo ribbon representation of the interaction between UPF3b and eIF4AIII (gray) (from complex 2) together with the 2fo-fc map, contoured at 1.0 s showing the electron density after UPF3b was modeled. The molecules are viewed in a similar orientation to that used in Fig. 2*C*. In addition, the electron density observed close to the conserved $Arg329_{eIF4A3}$ is shown, fitted with an Arg-Glu-Ala sequence. Notice that at this resolution it is not possible to assess the direction of the main chain for such a small segment of electron density, neither from the features of the electron density nor from the *R* free.

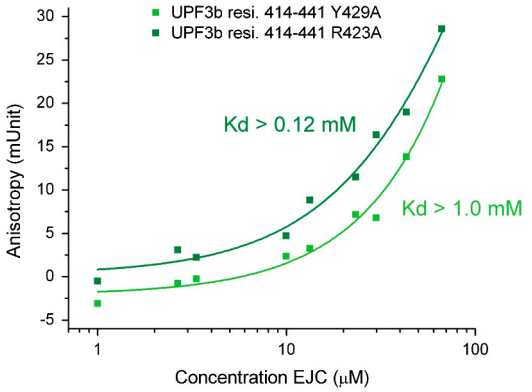

Fig. S4. Low-affinity binding between UPF3b mutated peptides and the EJC. Binding of the EJC to UPF3b mutated peptides (residues 414–441) Y429A or R423A in solution as measured by fluorescence anisotropy. The peptides were labeled with fluorescein at the carboxy terminus, and for labeling purposes a serine was introduced in place of the nonconserved cysteine residue at position 440. The affinity was determined as indicated in Fig. 3*C*.

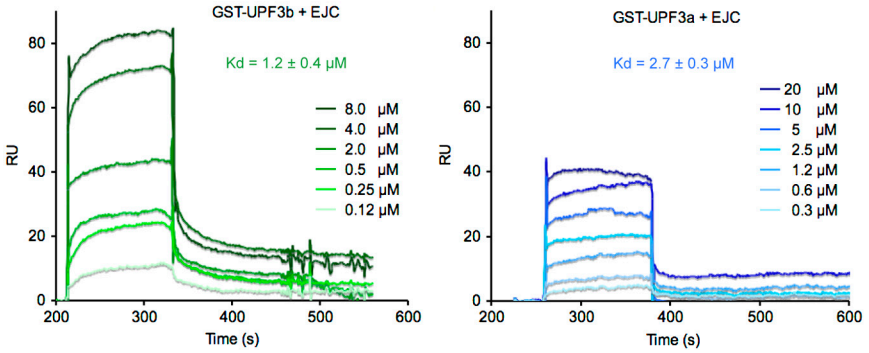

Fig. S5. Binding of the EJC to full-length UPF3b or UPF3a proteins as measured by surface plasmon resonance (BIAcore). Full-length GST-UPF3b (*Left*) and GST UPF3a (*Right*) were immobilized on chip surfaces coated with anti-GST antibody. Purified EJC was injected at different concentrations. The horizontal axis of the sensorgrams indicates the time (seconds) and the vertical axis indicates the RUs. Each dissociation constant (K_d) was obtained from at least four separate experiments and derived using a bimolecular interaction model.

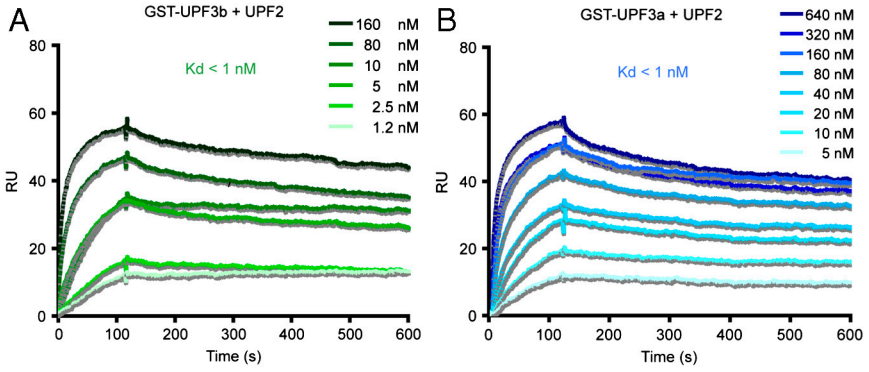

Fig. S6. High-affinity binding between UPF3 and UPF2. BIAcore analyses of UPF3 interactions showing affinities in the low nanomolar range for UPF2 binding. The experiments were carried out at 25 °C using a BIAcore 3000 (GE Healthcare). Full-length GST-UPF3 was immobilized on CM5 chip surfaces coated with anti-GST antibody. Approximately 10,000 RUs of anti-GST were immobilized using an amine coupling procedure with 30 μg/mL antibody at 5 μL per minute in 10 mM sodium acetate at pH 5.0. The anti-GST chips were then derivatized with 100–150 RUs of GST-tagged UPF3 in running buffer (40 mM Tris · HCl pH 7.5, 300 mM NaCl, and 1 mM DTT, 0.05% Tween 20). Purified UPF2 (residues 761–1227) was injected at different concentrations at a flow rate of 30 μL/ min in running buffer. An anti-GST flow cell was used as control. The horizontal axis of the sensorgrams indicates the time (seconds) and the vertical axis indicates the RUs. Each dissociation constant (K_d) was obtained from at least four separate experiments and derived using a bimolecular interaction model using the Origin software.

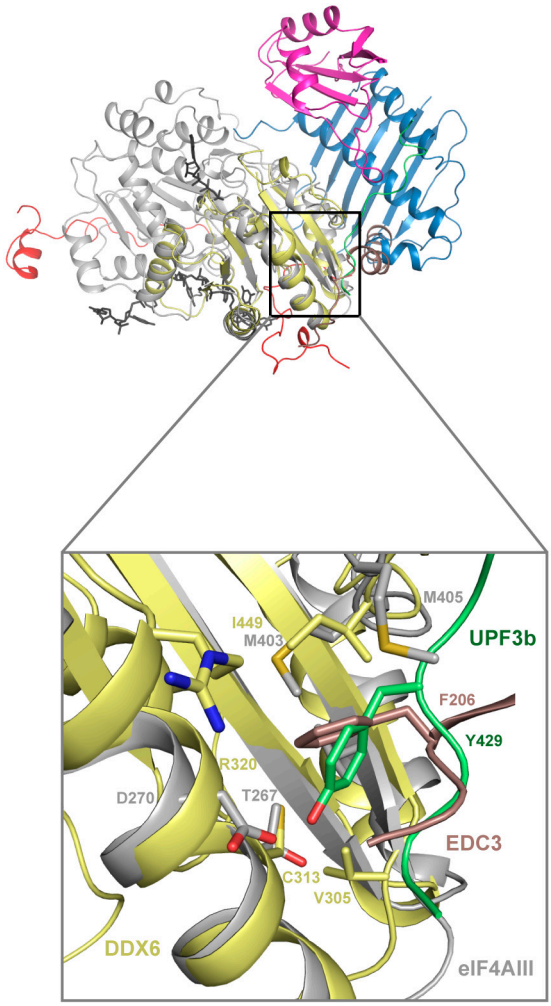

Fig. S7. Protein recognition at similar molecular surfaces. The surfaces of eIF4AIII (gray) and DDX6 (yellow) are shown (after optimal superimposition) bound to the corresponding interacting proteins, UPF3b and EDC3 (light brown). The close-up view shows the same structural position for $Tyr429_{UPF3b}$ and $Phe206_{EDC3}$. The structures are shown after optimal superimposition in the same orientation as in Fig. 4*A*.